Hydrogen transfer hydrogenolysis of organosolv Chinese fir lignin to monophenols over $NiZnAlO_x$ catalyst

Wenbing Yu [a], Chongbo Cheng [b,], Dekui Shen [a,*], Sai Gu [c], Kai Hong Luo [d]*

a Key Laboratory of Energy Thermal Conversion and Control of Ministry of Education, School of Energy and Environment, Southeast University, Nanjing 210096, PR China

b Engineering Laboratory of Energy System Process Conversion and Emission Reduction Technology of Jiangsu Province, School of Energy & Mechanical Engineering, Nanjing Normal University, Nanjing 210046, PR China

c School of Engineering, University of Warwick, Coventry CV4 7AL, W Midlands, UK

d Department of Mechanical Engineering, University College London, London WC1E7JE, UK

E-mail: C. B. Cheng: 220130473@seu.edu.cn

D.K. Shen: 101011398@seu.edu.cn

ABSTRACT: Lignin is the only naturally renewable aromatized polymer consisting of several phenyl propane structures linked by C-O and C-C bonds, so lignin can be depolymerized into value-added chemicals or liquid fuels. In this study, the $M_5Zn_5AlO_x$ (M=Co, Ni and Cu) catalysts were obtained by co-precipitation method and then were used in organosolv lignin depolymerization. Among these catalysts, the $Ni_5Zn_5AlO_x$ catalyst possessed the largest surface area and abundant surface oxygen vacancies as well as strong acidic sites on the surface, giving the highest yield of monophenols (about 14.49 wt.%). The effect of Ni/Zn ratios on the lignin depolymerization was also investigated,

and it was found that the surface area and the proportion of surface oxygen vacancies and strong acidic sites of the $NiZnAlO_x$ catalysts increased and then decreased with the Ni/Zn ratios increasing. Similarly, the yield of monomeric compounds increased and then decreased with the Ni/Zn ratios increasing. The highest yield of monophenols was 17.18 wt.% obtained over the $Ni_3Zn_7AlO_x$ catalyst, which was a remarkable monomer yield from organosolv lignin. The 2D HSQC NMR of bio-oil revealed that the linkage bonds in lignin could be effectively broken over the $Ni_3Zn_7AlO_x$ catalyst. This study provided an effective route to obtain high-value chemicals from organosolv lignin under nickel-based catalysts.

KEYWORDS: Lignin, Hydrogenolysis, Monophenols, Mixed metal oxides, Hydrogen donor solvent

1. INTRODUCTION

With the overconsumption of fossil energy, lignocellulose from agricultural residues, forestry waste and crops has been extensively studied for its use as a raw material for bioenergy/fuel and biochemical products [1]. Lignocellulose is composed of cellulose, hemicellulose and lignin. Cellulose and hemicellulose can be used in industry for the production of biofuels and chemicals (such as ethanol, formic acid, and furfural) through pyrolysis and fermentation, etc [2]. Lignin is mainly made up of three phenolic structural units, guaiacyl structure (G-type), syringol structure (S-type) and p-hydroxybenzene structure (H-type), which is a renewable resource of phenolic compounds and can be used as an alternative to fossil fuel [3-4]. The structural units in lignin are randomly connected by

C-O and C-C bonds, where the C-O bonds containing β-O-4, α-O-4, 4-O-5 and so on, and the C-C bonds involving 5-5 and β-β, etc [5]. From the perspective of linkage bonds, lignin can be effectively utilized to produce aromatic compounds such as benzene, toluene and phenol for fuels and basic chemicals if the linkage bonds between structural units can be broken successfully. However, the complexity of the linkage bonds makes it difficult to depolymerize lignin effectively and becomes a bottleneck for lignin utilization [6-7]. Chinese fir is an important silvicultural species in northeastern China and is known for providing the richest timber material, with over 69 million hectares of Chinese fir planted [8]. Thus, Chinese fir has great potential for the production of valuable chemicals.

The current thermochemical conversion of lignin into fuels and platform chemicals includes pyrolysis [9], hydrolysis [10], oxidation [11] and hydrogenolysis [12-13]. Compared with other methods, hydrogenolysis reaction condition is milder and the reaction process is easier to control, leading to higher selectivity and yield of monomer products, and less coke formation [5]. Lignin hydrogenolysis is usually carried out at temperatures of 200-300°C and involves the use of hydrogen and/or hydrogen donor solvents. Compared with the problems of low atomic economy and high safety risks of hydrogen, hydrogen donor solvents (methanol [14-15], ethanol [2, 16], isopropanol [17-18] and formic acid [19-20], etc.) can also improve the solubility of lignin, which is more favorable for lignin hydrogenolysis [21].

Although some progress has been made in lignin hydrogenolysis, the cost and efficiency of lignin hydrogenolysis are still its main issues. To some degree, the use of catalysts can reduce the cost of lignin hydrogenolysis [3]. The precious metals of the platinum group (e.g., Ru, Pd and Pt) are the most studied catalysts due to their high

hydrogenation activity [22-23]. However, the high cost and low availability hinder their large-scale use in industry. Non-precious metal catalysts such as Cu, Fe, Ni and Co have exhibited excellent selectivity in the cleavage of C-O bonds of aryl ethers due to their inherent metallic nature [24-28]. Low-cost transition metal oxides also usually exhibit remarkable activity and high-stability [29]. For example, Huang et al. used $CuMgAlO_x$ mixed metal oxides as a catalyst for the one-step conversion of Soda lignin to aromatic-based compounds in supercritical ethanol [30]. Compared the catalytic function with Cu/MgO and Cu/γ-Al_2O_3, it was found that the mixed metal oxides CuMgAl-MMO catalyst exhibited the best catalytic performance when the content of Cu was 20% and the (Cu+Mg)/Al ratio was 4 [31]. In addition, Yan et al. found that the metal Cu was more efficient than CuO in the catalytic lignin conversion by using reduced CuMgAl-MMO [32]. Kong et al. used Cu/$CuMgAlO_x$ catalyst into the hydrogenolysis of lignin in supercritical methanol to obtain 37.76 C% monomeric compounds. The linkage bonds in lignin could effectively be broken and the deoxygenation hydrogenation reaction was catalyzed by Cu/$CuMgAlO_x$ catalyst [33]. These studies suggested that reduction can enhance the catalytic activity of metal oxides and they mainly focused on Cu-based catalysts. Moreover, it was reported that Co, Ni, Cu and Zn as transition metal elements have d orbitals that can polarize hydrogen, showing better catalytic performance in experimental studies of the hydrogenolysis of lignin [34-35].

In this study, mixed metal oxides M_5Zn_5Al-MMO (M=Co, Ni and Cu) were prepared by co-precipitation method and then reduced under H_2 atmosphere to obtain $M_5Zn_5AlO_x$ (M=Co, Ni and Cu) catalysts, which were further used into the hydrogenolysis of lignin

in a mixed ethanol/isopropanol solvent as hydrogen-donors in order to investigate the catalytic performance of different active centers (Co, Ni and Cu). Then, the catalytic performance of the catalysts with different Ni/Zn ratios for hydrogen transfer hydrogenolysis of lignin was investigated. The specific surface area and the amount of surface oxygen vacancies and acidic sites were adjusted by altering Ni/Zn ratios in the catalysts. Finally, the possible reaction pathway was speculated by analyzing monophenols and bio-oil obtained from the reaction.

2. MATERIALS AND METHODS

2.1. Materials and chemicals. Lignin was extracted from Chinese fir, according to literature[36]. Chinese fir was ground close to 0.5 mm, extracted with ethanol and toluene (1:1 v/v) to remove impurities such as waxes on the surface, washed and dried. 50 g of wood was then extracted in 625 ml of formic acid/acetic acid/water (3:5:2 v/v/v) at 110 °C for 6 h. The product was filtered and spun under reduced pressure to a brownish-red mucilage, added with excess water, filtered and washed to neutral. The filter residue was dried to obtain Chinese fir lignin. All chemicals which were used in the experiments were purchased from Sinopharm Chemical Reagent Co. They were of analytical grade. Nitrogen (99.999%) was provided by Nanjing Shangyuan Industrial Gas Co.

2.2. Catalyst preparation method. According to literature [30], nickel-based catalyst preparation process as a typical process, $Ni(NO_3)_2•6H_2O$, $Zn(NO_3)_2•6H_2O$ and $Al(NO_3)_3•9H_2O$ (n (Ni^{2+}): n (Zn^{2+})=5: 5, n (M^{3+}): n (M^{2+}+M^{3+})=1: 3) were dissolved in 100 ml of deionized water. NaOH was dissolved in 100 ml of deionized water and

Na_2CO_3 was dissolved in 250 ml of deionized water. The metal nitrate solution and aqueous NaOH solution were dropped slowly together into aqueous Na_2CO_3 solution and maintained pH = 10 with stirring at 60 °C. At the end of the titration (about 45 min), the slurry was aged at 60 °C with stirring for 24 hours. The precipitate was filtered and washed with deionized water until the pH=7 of the filtrate. The solid was dried at 105 °C overnight and grinded into less than 125 μm particles. The solid was calcined at 460 °C (heating rate 2 °C/min) under air atmosphere for 6 h to obtain metal oxides marked as Ni_5Zn_5Al-MMO. Finally, the temperature of the tube furnace increased from 460 °C to 600 °C at a heating rate of 5 °C/min. The catalyst precursor was reduced under 80 mL/min of nitrogen containing 20% v/v hydrogen for 2 h and then cooled to room temperature to obtain the catalyst, marked as $Ni_5Zn_5AlO_x$. $Co_5Zn_5AlO_x$ and $Cu_5Zn_5AlO_x$ were prepared in the same way. In order to compare the catalytic performance of catalysts with different Ni/Zn ratios, the catalysts were prepared using the same method with n (Ni^{2+}): n (Zn^{2+}) = y: 10-y (y=0, 1, 3, 5, 7, 9 and 10) and n (M^{3+}): n (M^{2+}+ M^{3+}) =1: 3.The catalysts were labeled as $Ni_yZn_{10-y}AlO_x$. The chemical compositions of catalysts were further verified by the ICP analysis (Table S3).

2.3. Lignin hydrogenolysis processing. Lignin hydrogenolysis experiment was conducted in a stainless steel reactor (SLM50, Beijing Century Senlong Experimental Instruments Co.). In a typical run, 150 mg of lignin, 50 mg of catalyst and 30 mL of ethanol/isopropanol (1:1 v:v) solvent were mixed, then 20 μL of n-decane was added as an internal standard, and the quartz liner was placed in stainless steel reactor. The reactor was closed and purged 5 times with N_2. The reaction vessel was then pressurized to 1

MPa N_2 at room temperature and the experiment was carried out at 270 °C for 4 h under continuous stirring (400 rpm). The reaction reactor was cooled to room temperature in a water bath, then the mixture was filtered. The filter residues were washed three times with ethanol, and the catalyst was separated from the coke by using the magnetic properties of the catalyst. The coke was then dried at 105°C overnight. The liquid was fixed to 50 ml with ethanol, and 1 ml of the liquid phase product was taken for the qualitative and quantitative analysis of monophenolic compounds. By spinning under vacuum, the solvent in the remaining liquid was removed to obtain bio-oil.

2.4. Structural properties of catalysts. Brunner-Emmet-Teller (BET) measurement was used to obtain pore structure information. The measurement was carried out using an Autosorb-IQ2 nitrogen physisorption apparatus, and then nitrogen desorption experiment was performed in 77k liquid nitrogen. X-ray diffraction (XRD) was used to analyze crystal phase composition of catalysts. The measurement was performed using a Nihon Rei Smartlab (3) X-ray powder diffractometer with a 3KW X-ray generator and Cu target with a CBO crossover optical path. It recorded in 0.02° steps in the angular range of 10-80°, with a scanning speed of 3°/min. X-ray photoelectron spectrometer (XPS) was used to characterize the chemical valence of the surface elements of catalysts. The measurement was carried out on a PreVac XPS-2. NH_3-temperature programmed desorption (NH_3-TPD) was used to measure the distribution of acidic sites on the catalyst surface, which was carried out with AutoChem II 2920 with a heating-up procedure: after purging for 10 min under He atmosphere (flow rate of 30 mL/min), heating from room temperature to 500 °C at a heating rate of 15 °C/min, followed by holding treatment for

1 h; cooling to 100 °C at a cooling rate of 10 °C/min. Adsorption at 100 °C using a 5% NH_3-95% He mixture (flow rate of 30 mL/min) to a smooth baseline. After saturation of adsorption at 100 °C, purging to a smooth baseline using He (flow rate of 30 mL/min). Starting the programmed heating-up and recording data under He (flow rate of 30 mL/min) atmosphere to 700 °C at a heating-up rate of 10 °C/min, followed by holding for 30 min. Afterwards, the test was ended by cooling down to room temperature under He (flow rate of 10 mL/min) atmosphere. Scanning electron microscope (SEM) was utilized to observe the catalyst micromorphology, performed on a Zeiss Sigma 300 with a Smart EDX. Transmission electron microscope (TEM) was applied to characterize the catalyst microstructure with JEM 2100F.

2.5. Characterizations of lignin hydrogenolysis products. Gas chromatography-mass spectrometry (GC-MS) and hydrogen ion flame gas chromatography (GC-FID) were used for the qualitative and quantitative analysis of monophenols from lignin depolymerization. The qualitative analysis was performed on a Thermo ITQ 1100 equipped with an HP5MS (30m * 0.25mm * 0.25μm) column with a heating-up procedure: hold at 50 °C for 3min, raise up to 250 °C at 10°C / min and maintain at 250 °C for 5min. The quantitative analysis was performed on a GC 3900 equipped with an HP5MS (30m * 0.25mm * 0.25μm) column. The quantification of monophenols was performed by the effective carbon number method using n-decane as the internal standard [37]. Two-dimensional ^{1}H-^{13}C heteronuclear single-quantum coherence NMR spectroscopy (2D HSQC NMR) was used to characterize the changes of linkage bonds in lignin and bio-oil. NMR measurements of lignin or bio-oil were recorded using a Bruker AVANCE III HD 600 MHz instrument.

Lignin or bio-oil was dissolved in deuterated dimethyl sulfoxide (DMSO-d_6). MestReNova software was used for data processing. Gel permeation chromatography (GPC) was used to determine the relative molecular mass of lignin and bio-oil. Lignin or bio-oil was dissolved in 2 ml of tetrahydrofuran (THF) and then analyzed by PL-GPC220 (Polymer Laboratories). The mobile phase (THF) flow rate was 0.7 ml/min and polystyrene was used as the standard curve. Mass yields of monomeric phenols detected by GC-MS were calculated as

$$Y = M_{monophenols} / M_{lignin} \times 100\% \quad (1)$$

where $M_{monophenols}$ is the mass of monomeric phenols, and M_{lignin} is the mass of starting lignin.

3. RESULTS AND DISCUSSION

3.1. Structural characterization of catalysts. The parameters of the catalyst pore structure were shown in Table 1. The Ni_5Zn_5Al-MMO had the largest pore volume and pore size of 1.56 cm^3/g and 28.70 nm, respectively. After reduction, the pore volume and pore size of the $Ni_5Zn_5AlO_x$ catalyst reduced, while the BET surface area increased to 241.56 m^2/g, which may be due to the fact that the high reduction temperature changed the pore structure of the catalyst. This was consistent with the figure of adsorption-desorption isotherms of Ni_5Zn_5Al-MMO and $Ni_5Zn_5AlO_x$ (Figure S1). Among the $M_5Zn_5AlO_x$ (M=Ni, Co and Cu) catalysts, the BET surface area, pore volume and pore diameter of the $Ni_5Zn_5AlO_x$ catalyst were the largest. In addition, the parameters of pore structure first increased and then decreased with the Ni/Zn ratios of the $Ni_yZn_{10-y}AlO_x$

catalyst increasing. The maximum BET surface area and pore volume were the Ni/Zn ratio of 5:5. Lager BET surface area and pore volume of the catalysts would be beneficial to the dispersion of the active components and the diffusion of the reactants in the pores, improving the catalytic activity of catalysts [38].

Table 1 BET surface area, pore volume and pore size of catalysts

	BET surface area (m^2/g)	Pore volume [a] (cm^3/g)	Pore size [b] (nm)
Ni_5Zn_5Al-MMO	208.61	1.56	28.70
$Ni_5Zn_5AlO_x$	241.56	1.32	18.61
$Co_5Zn_5AlO_x$	153.49	0.52	16.10
$Cu_5Zn_5AlO_x$	168.85	0.18	15.00
$Zn_{10}AlO_x$	114.13	0.24	16.40
$Ni_1Zn_9AlO_x$	161.87	0.68	21.26
$Ni_3Zn_7AlO_x$	184.04	1.04	23.60
$Ni_7Zn_3AlO_x$	195.62	1.21	14.91
$Ni_9Zn_1AlO_x$	194.66	0.98	12.44
$Ni_{10}AlO_x$	168.32	1.02	10.40

[a] Single point adsorption total pore volume of pores

[b] BJH desorption average pore diameter

The crystal phase compositions of catalysts were obtained by XRD analysis, as shown in Figure 1. The peaks of ZnO (Zn^{2+}) and NiO (Ni^{2+}) could be observed in the Ni_5Zn_5Al-MMO, however, no signals of Al_2O_3 appeared, which was probably due to the presence

of amorphous Al_2O_3 in the catalyst [39]. In the $Ni_5Zn_5AlO_x$ catalyst, the distinct peaks of Ni could be observed at 2θ=44.51°, 51.85° and 76.37°, which showed that NiO in the Ni_5Zn_5Al-MMO was reduced to metal Ni. In addition, spinel phases mainly composed of $ZnAl_2O_4$ were also observed, which came from metal oxides as a result of high temperature reduction [40]. In the $Co_5Zn_5AlO_x$ and $Cu_5Zn_5AlO_x$ catalysts, Co (111), (200) and (220) crystalline surfaces could be observed, and signals of Cu were observed at 2θ = 43.29°, 50.43° and 74.13°, which indicated the appearance of metal Co and Cu, respectively. The spinel phases were also observed in the catalysts after reduction. As the Ni/Zn ratios increased in the $Ni_yZn_{10-y}AlO_x$ catalyst, the phase composition of catalysts changed from the initial ZnO and Al_2O_3 to Ni, ZnO and spinel phases, and further changed to Ni and spinel phases. When the catalyst was free of Zn, the catalyst was composed of Ni, Al_2O_3 and NiO. In addition, with the higher intensity of spinel phases, the catalyst possessed larger BET surface area and pore volume.

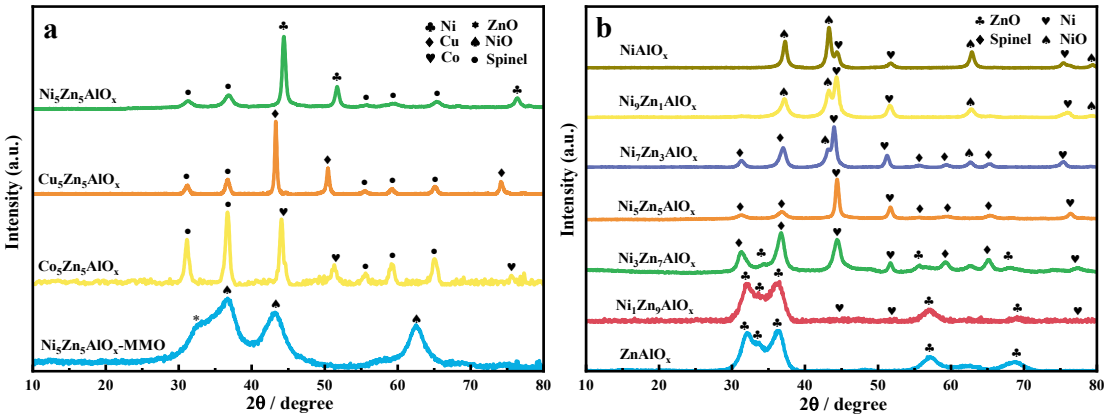

Figure 1 XRD patterns of $M_5Zn_5AlO_x$ (M=Ni, Co and Cu) catalysts (a) and $Ni_yZn_{10-y}AlO_x$ catalysts (b)

The XPS patterns of the catalysts were shown in Fig. 2. In the Ni_5Zn_5Al-MMO catalyst, Ni^{2+} for Ni $2p_{3/2}$ (854.56 eV) and $Ni2p_{1/2}$ (873.28 eV) were observed, which was assigned

to the formation of NiO [24]. The ratio of Ni^{2+} to the number of atoms on the catalyst surface was about 4.98%. The signal peaks Zn^{2+} in ZnO of $Zn2p_{3/2}$ and $Zn2p_{1/2}$ appeared at 1021.58 eV and 1044.6 eV, respectively [41], and the signal peaks (74.01eV) of Al 2p was attributed to Al^{3+} in Al_2O_3 [41]. In the spectrum of the $Co_5Zn_5AlO_x$ catalyst, Co^0 and Co^{2+} accounted for 3.35% and 1.88% on the catalyst surface, respectively. For the $Cu_5Zn_5AlO_x$ catalyst, Cu^0 and Cu^{2+} accounted for 2.53% and 1.34%, respectively. In the spectrum of the $Ni_5Zn_5AlO_x$ catalyst, Ni^0 and Ni^{2+} constituted 2.13% and 1.01%, respectively. The percentage of Al in the number of atoms on the catalyst surface was about 28.2%. The increased Al content on the catalyst surface compared to the unreduced metal oxides (17.64%) implied that Al migrated to the catalyst surface under high reduction temperatures. It was reported that the presence of Al_2O_3 could affect the activity and selectivity of Ni in the catalyst by spatial site resistance effect [42]. Two peaks of O 1S appeared at 530.1 eV and 531.7 eV, respectively, which could be attributed to the lattice oxygen and to the oxygen atoms near the oxygen vacancies on the surface of the catalyst after reduction [43]. For the $Ni_yZn_{10-y}AlO_x$ catalysts, the proportion of surface oxygen vacancies based on the semi-quantitative analysis of XPS first increased and then decreased with the increasing of Ni/Zn ratios, and the highest proportion of surface oxygen vacancies was obtained when Ni/Zn was 5:5. The binding energy of Ni $2p_{3/2}$ for Ni^0 increased from 853.13 eV in $Ni_9Zn_1AlO_x$ to 853.51 eV in $Ni_3Zn_7AlO_x$, and the binding energy of Zn $2p_{3/2}$ for Zn^{2+} decreased, indicating that some electrons were transferred from Ni to Zn, leading to a decrease in the electron cloud density of Ni, which was favorable to the breakage of C-O bonds (Figure 2c and 2d) [44].

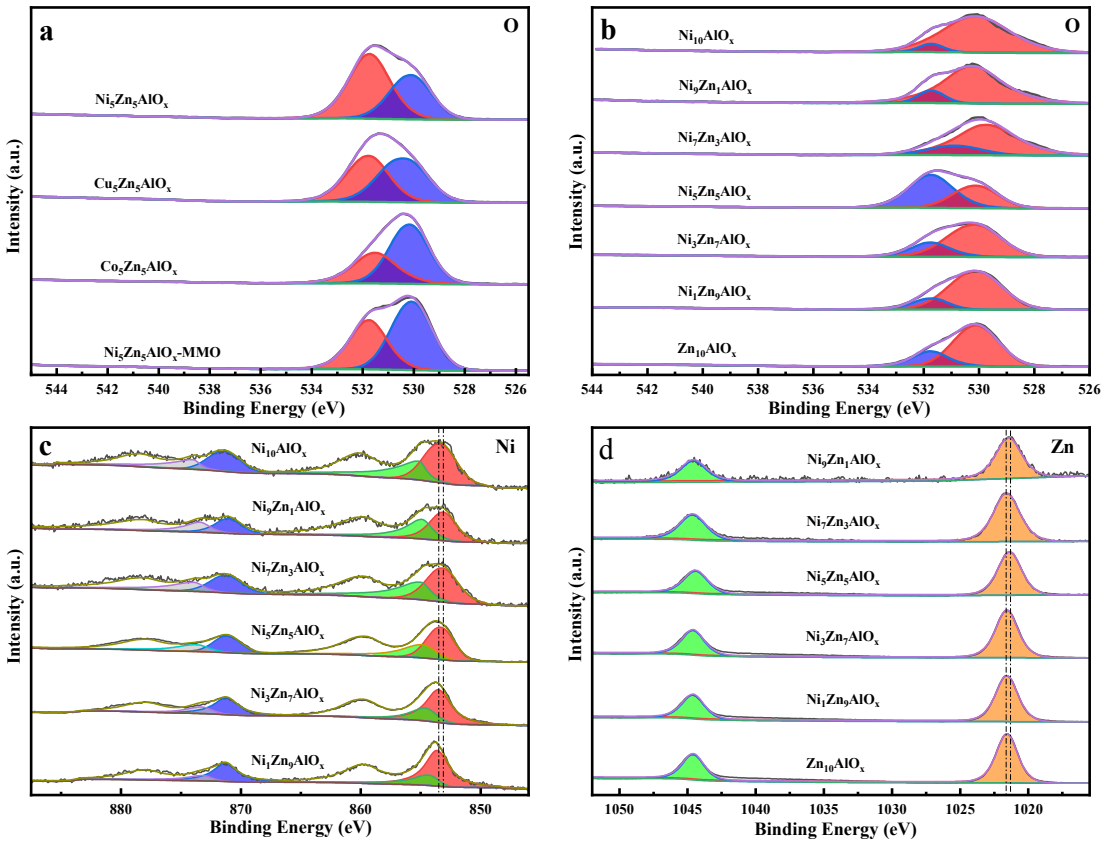

Figure 2 XPS analysis of binding energy of oxygen element in $M_5Zn_5AlO_x$ (M=Ni, Co and Cu) catalysts (a) and binding energy of oxygen element (b), nickel element (c) and zinc element (d) in $Ni_yZn_{10-y}AlO_x$ catalyst

The distribution of acidic sites in the catalysts was obtained by NH_3-TPD analysis, as shown in Figure 3. The acid sites could be divided into three types: (i) weak acids at the low temperature region (300 °C and below); (ii) medium acids at the medium temperature region (300-500 °C); and (iii) strong acids at the high temperature region (500 °C and above) [45]. In the Ni_5Zn_5Al-MMO, the peaks of acidic sites appeared with 47.50% of weak acidic sites and 37.80% of medium acidic sites. The acidic sites of the $Co_5Zn_5AlO_x$ and $Cu_5Zn_5AlO_x$ catalyst were dominated by medium acidic sites, accounting for 45.56% and 57.37%, respectively. Compared with Ni_5Zn_5Al-MMO, the peaks of the $Ni_5Zn_5AlO_x$ catalyst shifted toward to the higher temperature, which indicated that the enhanced

acidity of the catalyst after reduction. This might be related to the spinel phase in the reduced catalyst. Among the catalysts with different Ni/Zn ratios, the catalyst acidity first enhanced and then weakened with the increasing of Ni/Zn ratio, and the highest percentage (about 58.40%) of strong acid sites was obtained on the $Ni_5Zn_5AlO_x$ catalyst. This was positively correlated with the proportion of spinel phase in catalysts, indicating that the larger amount of spinel phase, the stronger acidity of catalysts.

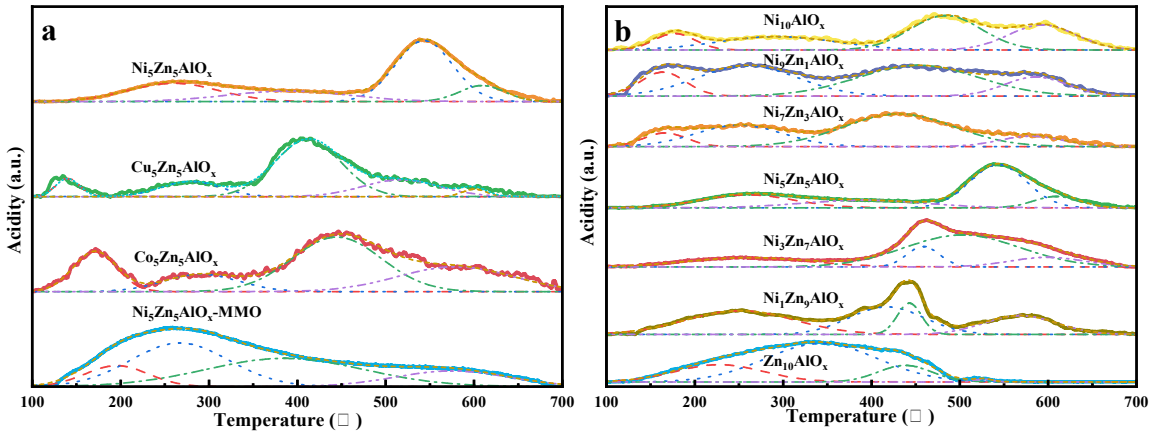

Figure 3 NH_3-TPD profiles of $M_5Zn_5AlO_x$ (M=Ni, Co and Cu) catalysts (a) and $Ni_yZn_{10-y}AlO_x$ catalysts (b)

The microscopic morphology of the $Ni_3Zn_7AlO_x$ catalyst was obtained by SEM and TEM analysis, as shown in Figure 4. The microscopic morphology of the catalyst showed a flocculent structure as observed in SEM image (Figure 4a). Combined with the SEM-mapping pattern (Figure 4b), it could be observed that the nickel, zinc, aluminum and oxygen elements in the catalyst were uniformly distributed on the catalyst surface, implying the good dispersion of active particles. The statistical analysis of the catalyst particle size exhibited that the average particle size of nickel metal was 15.85 nm as showing in TEM image (Figure 4c). The lattice spacing of 0.176 nm for Ni (200), 0.286 nm for spinel $ZnAl_2O_4$ (220) and 0.248 nm for ZnO (101) were clearly observed in the

TEM (Figure 4d), which were also consistent with the catalyst composition observed by XRD.

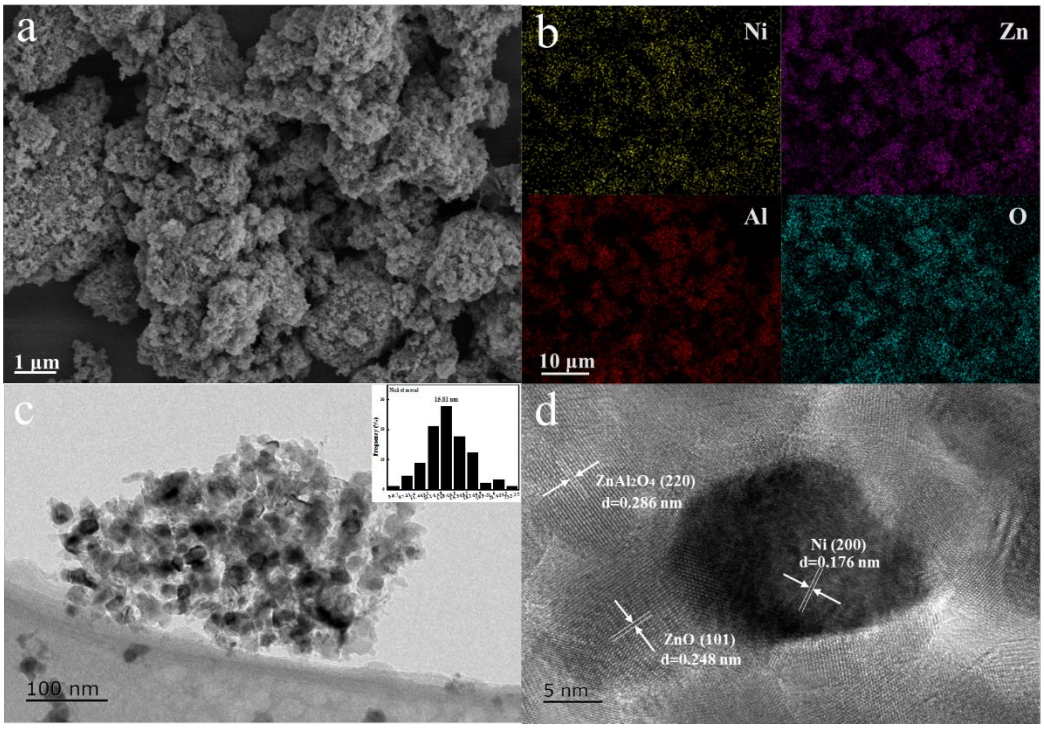

Figure 4 SEM image (a), SEM-mapping (b), TEM image (c) and Ni crystalline planes (b) of $Ni_3Zn_7AlO_x$ catalyst

3.2. Product yields from catalytic hydrogenolysis of lignin. The yields of monophenols from the hydrogen transfer hydrogenolysis of lignin with different catalysts were shown in Figure 5. Without catalyst, the hydrogenolysis of lignin yielded 8.07 wt.% monophenols. No obvious change of the monophenols yield from the lignin hydrogenolysis over the Ni_5Zn_5Al-MMO was found, indicating the low catalytic activity of the unreduced metal oxides. The yield of monophenols enhanced under the $Co_5Zn_5AlO_x$, $Cu_5Zn_5AlO_x$ and $Ni_5Zn_5AlO_x$ catalyst, respectively (Figure 5a). The best catalytic performance was shown under the $Ni_5Zn_5AlO_x$ catalyst, in which the lignin hydrogenolysis produced 14.49 wt.% monophenols, which could be attributed to the

larger specific surface area, abundant surface oxygen vacancies and strong acid sites on the $Ni_5Zn_5AlO_x$ catalyst. The C-C bonds in lignin were preferentially broken by the activation of the acid sites in catalysts [46].In addition, the monomeric products were dominated by side-chain-free and ternary carbon atomic side chains over the Ni_5Zn_5Al-MMO, while the proportion of ternary side-chain monophenols increased significantly and the proportion of side-chain-free compounds decreased over the $Ni_5Zn_5AlO_x$ catalyst (shown in Table S1). The $Ni_5Zn_5AlO_x$ catalyst had a good selectivity for ternary side-chain monophenols.

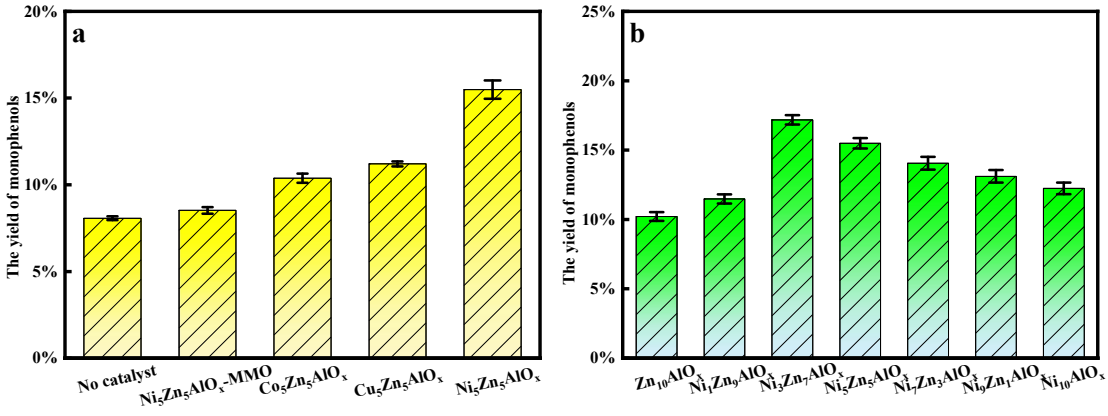

Reaction condition: 0.15g linin, 0.05g catalyst, 30 mL ethanol/isopropanol (1:1 v: v), 270 °C, 4 h

Figure 5 Yield distributions of monophenols obtained from hydrogenolysis of lignin on $M_5Zn_5AlO_x$ (M=Ni, Co and Cu) catalysts (a) and $Ni_yZn_{10-y}AlO_x$ catalysts (b)

Since the catalytic activity of $Ni_5Zn_5AlO_x$ was superior to that of $Co_5Zn_5AlO_x$ and $Cu_5Zn_5AlO_x$ catalyst, the different Ni/Zn ratios of catalysts were further investigated in lignin hydrogenolysis (shown in Figure 5b). The $Zn_{10}AlO_x$ catalyst produced the lowest yield of monophenols, indicating that nickel play an important role in the catalytic hydrogenolysis of lignin. The yield of monophenols first increased and then decreased

with the increasing nickel content, which was consistent with the change of the catalyst specific surface area and the amount of surface oxygen vacancies as well as strong acid sites. The highest yield of monophenols obtained from the lignin hydrogenolysis was about 17.18 wt.% over the $Ni_3Zn_7AlO_x$ catalyst. The Zn element in the catalyst favored the adsorption of lignin fragments containing C=O bonds on the catalyst surface, and the substrate was protonated and activated by the acidic sites of the catalyst [29]. With the increasing of Ni/Zn ratios, the yields of eugenol and isoeugenol (had unsaturated side chains) first increased and then decreased, indicating that at low Ni/Zn ratios, the reaction was dominated by catalytic hydrogenolysis; when at high Ni/Zn ratios, Ni atoms promoted the hydrogenation reaction to some extent. The stability of the $Ni_3Zn_7AlO_x$ catalyst for the depolymerization of lignin was also investigated. The yield of monophenols was 17.18 wt.% in the first test. The results indicated that the yield of monophenols almost no obvious change after five consecutive runs (shown in Figure S2), demonstrating the excellent stability of $Ni_3Zn_7AlO_x$.

3.3. 2D HSQC MNR analysis of bio-oil. The 2D HSQC NMR spectra of lignin and bio-oil derived from catalytic hydrogenolysis over the $Ni_3Zn_7AlO_x$ catalyst were shown in Figure 6. The 2D HSQC NMR spectra can be divided into two regions: the aromatic region (δC/δH 100-135/5.5-8.5) and the side chain region (δC/δH 50-90/2.5-6.0) [47]. In the side chain region, three major linkage bonds were clearly observed in lignin: β-O-4 (A), β-5 (B) and β-β (C), where the most abundantly distributed linkage bond was β-O-4. The signals of the G-type structure, S-type structural unit and FA-type structure were still observed in the aromatic region of bio-oil from the lignin hydrogenolysis over the

$Ni_3Zn_7AlO_x$ catalyst, but the intensity of the corresponding peaks was declined. The appearing of the H-type unit in the bio-oil indicated that the demethoxylation reaction was promoted by the $Ni_3Zn_7AlO_x$ catalyst. In the side chain region, the β-O-4, β-5 and β-β bonds were invisible, indicating that the β-O-4, β-5 and β-β bonds in lignin were more likely to be broken over the $Ni_3Zn_7AlO_x$ catalyst. GPC analysis (Table S5) also confirmed that lignin was effectively depolymerized over the $Ni_3Zn_7AlO_x$ catalyst.

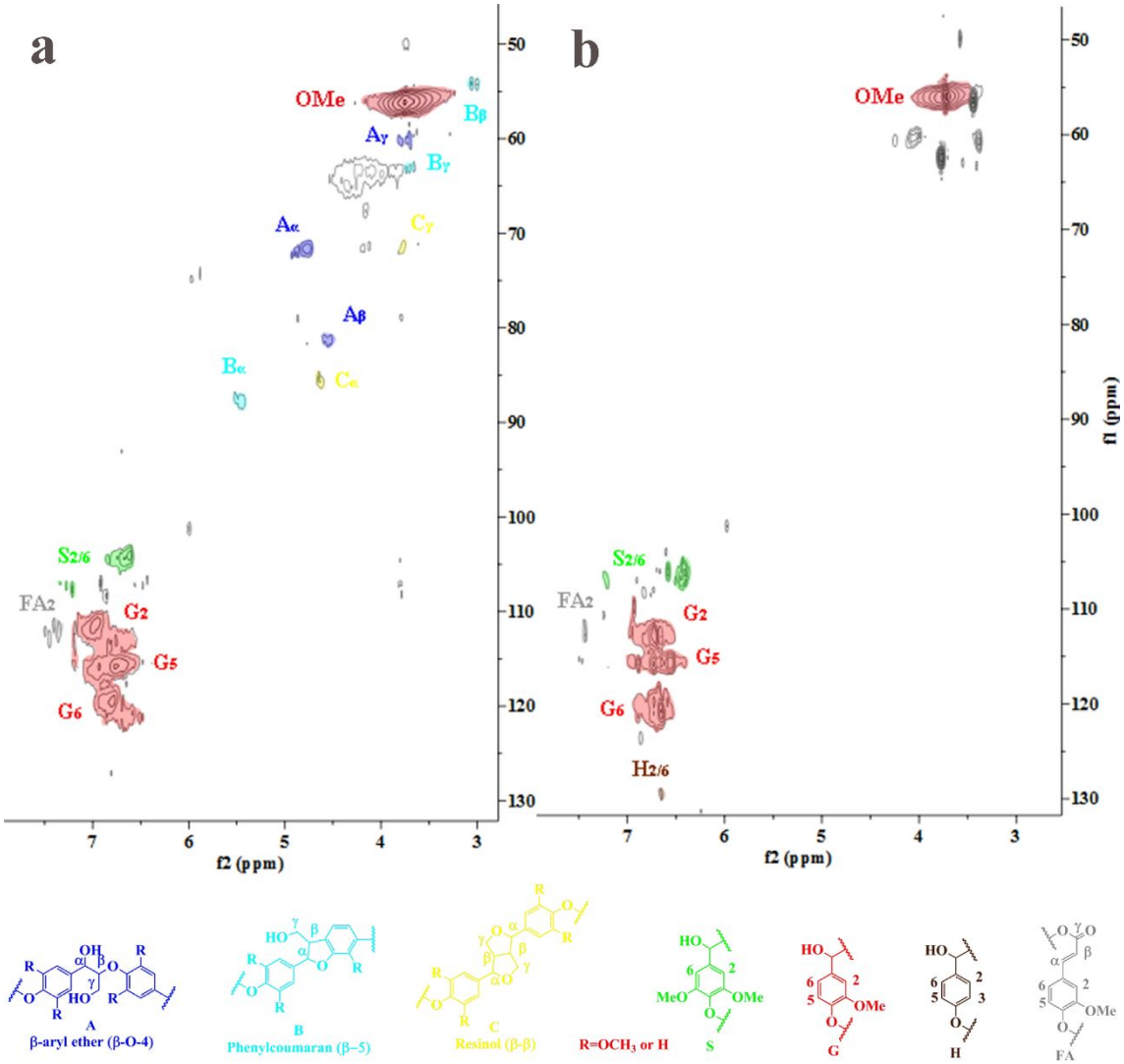

Figure 6 2D HSQC MNR of lignin (a) and bio-oil with the $Ni_3Zn_7AlO_x$ catalyst (b)

3.4. Plausible reaction pathways for the catalytic hydrogenolysis of lignin. A possible reaction pathway for the hydrogenolysis of lignin over the $Ni_3Zn_7AlO_x$ catalyst was

speculated by combining the analysis of the study results, which was shown in Figure 7. First of all, the dehydrogenation reaction of ethanol and isopropanol catalyzed by nickel and acidic sites on the catalyst generated aldehydes and hydrogen atoms [48], and the hydrogen radicals *in situ* participated in the lignin hydrogenolysis. Then, the oxygen-containing functional groups in lignin interacted with oxygen vacancies and zinc particles on the catalyst surface [29]. The lignin adsorbed on the catalyst surface was activated by acidic sites and catalyzed by nickel to yield enol ether intermediates by protonation of -OH in lignin [49]. The intermediates were further depolymerized to generate monophenolic compounds, while a portion of the intermediates containing benzyl cations might be attacked by other aromatic nuclei during the reaction process, resulting in condensation reaction. At the same time, monophenols containing unsaturated side chains such as eugenol and isoeugenol further underwent hydrogenation reactions over nickel atoms.

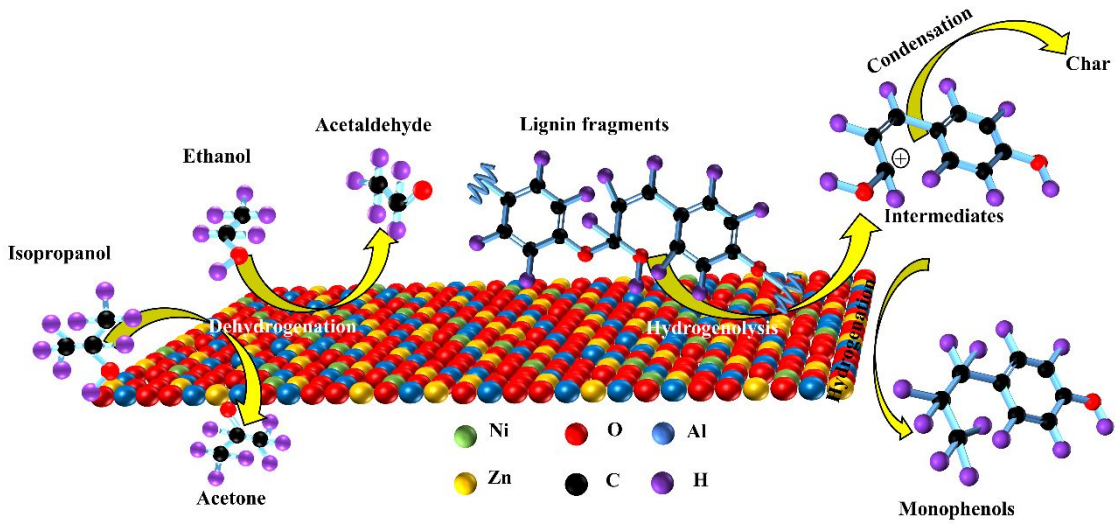

Figure 7 Plausible reaction pathway for the catalytic hydrogenolysis of lignin

4. CONCLUSIONS

The catalytic depolymerization of organosolv lignin over inexpensive mixed metal catalysts to monophenolic compounds was investigated. $M_5Zn_5AlO_x$ (M=Co, Ni and Cu) catalysts were obtained by co-precipitation method. Compared with the reduced catalyst, BET surface area of Ni_5Zn_5Al-MMO was smaller, and the proportion of weak acidic sites was larger. Among these catalysts, $Ni_5Zn_5AlO_x$ had the largest BET surface area (241.56 m^2/g) and the largest proportion of oxygen vacancies and strong acidic sites on the surface. Lignin was depolymerized in ethanol/isopropanol with $Ni_5Zn_5AlO_x$ to monophenols with the highest yield about 14.49 wt.%, and the ternary carbon side chain compounds dominated the monomer compounds, so $Ni_5Zn_5AlO_x$ exhibited superior selectivity for ternary side chain monophenols. The study further investigated the relationship between different Ni/Zn ratios in catalysts and the lignin depolymerization efficiency. With the increase of Ni/Zn ratios, the BET surface area and the amount of oxygen vacancies and strong acidic sites on the catalyst surface increased and then decreased. Similarly, the yields of monophenols from lignin depolymerization increased and then decreased, where up to 17.18 wt.% of the monomer products was obtained over the $Ni_3Zn_7AlO_x$ catalyst. By the 2D HSQC NMR of bio-oil, it was found that the catalyst could effectively catalyze the reaction of breaking the major linkage bonds in lignin. The dehydrogenation of ethanol and isopropanol catalyzed by nickel atoms in $Ni_3Zn_7AlO_x$ was accompanied by the depolymerization of lignin to obtain monophenols by the coordinated action of strong acidic sites on the catalyst surface and nickel atoms. This research provides a reliable method for high value utilization of lignin.

ASSOCIATED CONTENT

Supporting Information

Monophenols yields from hydrogenolysis of lignin on $M_5Zn_5AlO_x$ (M=Ni, Co and Cu) catalysts and $Ni_yZn_{10-y}AlO_x$ catalysts; chemical compositions of the catalysts; the catalytic properties and performances of the catalysts; relative molecular masses of lignin and bio-oil; the yield of bio-oil and coke; adsorption-desorption isothems of Ni_5Zn_5Al-MMO and $Ni_5Zn_5AlO_x$; and the stability of the $Ni_3Zn_7AlO_x$ catalyst for lignin hydrogenolysis.

AUTHOR INFORMATION

Corresponding Authors

*E-mail: 220130473@seu.edu.cn (C. B. Cheng); 101011398@seu.edu.cn (D.K. Shen)

Notes

The authors declare no competing financial interest.

ACKNOWLEDGEMENTS

The authors gratefully acknowledge the financial support from the Natural Science Research Project in Colleges and Universities of Jiangsu Province, China (grant number: 21KJB480004), National Natural Science Foundation of China (grant numbers. 51861145102) and the Key Research & Development Program of Jiangsu Province (grant number: BE2020114).

REFERENCES

1. Wang, D.; Li, G.; Zhang, C.; Wang, Z.; Li, X., Nickel nanoparticles inlaid in lignin-derived carbon as high effective catalyst for lignin depolymerization. *Bioresource Technology* **2019,** *289*, 121629.
2. Yuan, Z.; Cheng, S.; Leitch, M.; Xu, C., Hydrolytic degradation of alkaline lignin in hot-compressed water and ethanol. *Bioresource Technology* **2010,** *101* (23), 9308-9313.
3. Liu, B.; Du, B.; Sun, Y.; Zhu, M.; Yang, Y.; Wang, X.; Zhou, J., Ultrasound acoustic cavitation enhances depolymerization of organosolv lignin to phenolic monomers and low molecular weight lignin bio-oils. *Fuel Processing Technology* **2020,** *203*, 106387.
4. Shao, L.; Zhang, Q.; You, T.; Zhang, X.; Xu, F., Microwave-assisted efficient depolymerization of alkaline lignin in methanol/formic acid media. *Bioresource Technology* **2018,** *264* (10), 238-243.
5. Totong, S.; Daorattanachai, P.; Laosiripojana, N.; Idem, R., Catalytic depolymerization of alkaline lignin to value-added phenolic-based compounds over Ni/CeO2-ZrO2 catalyst synthesized with a one-step chemical reduction of Ni species using NaBH4 as the reducing agent. *Fuel Processing Technology* **2020,** *198* (10), 106-248.
6. Huang, X.; Atay, C.; Zhu, J.; Palstra, S. W. L.; Korányi, T. I.; Boot, M. D.; Hensen, E. J. M., Catalytic Depolymerization of Lignin and Woody Biomass in Supercritical Ethanol: Influence of Reaction Temperature and Feedstock. *ACS Sustainable Chemistry & Engineering* **2017,** *5* (11), 10864-10874.
7. Zhao, L.; Ouyang, X.; Ma, G.; Qian, Y.; Qiu, X.; Ruan, T., Improving antioxidant activity of lignin by hydrogenolysis. *Industrial Crops and Products* **2018,** *125* (5), 228-235.
8. Yu, H.; Guo, G.; Zhang, X.; Yan, K.; Xu, C., The effect of biological pretreatment with the selective white-rot fungus Echinodontium taxodii on enzymatic hydrolysis of softwoods and hardwoods. *Bioresour Technol* **2009,** *100* (21), 5170-5.
9. Yeo, J. Y.; Chin, B. L. F.; Tan, J. K.; Loh, Y. S., Comparative studies on the pyrolysis of cellulose, hemicellulose, and lignin based on combined kinetics. *Journal of the Energy Institute* **2019,** *92* (1), 27-37.
10. Jia, Y.; Yang, C.; Shen, B.; Ling, Z.; Huang, C.; Li, X.; Lai, C.; Yong, Q., Comparative study on enzymatic digestibility of acid-pretreated poplar and larch based on a comprehensive analysis of the lignin-derived recalcitrance. *Bioresour Technol* **2021,** *319*, 124225.
11. Liu, C.; Wu, S.; Zhang, H.; Xiao, R., Catalytic oxidation of lignin to valuable biomass-based platform chemicals: A review. *Fuel Processing Technology* **2019,** *191*, 181-201.
12. Cheng, C.; Li, P.; Yu, W.; Shen, D.; Jiang, X.; Gu, S., Nonprecious Metal/Bimetallic Catalytic Hydrogenolysis of Lignin in a Mixed-Solvent System. *ACS Sustainable Chemistry & Engineering* **2020,** *8* (43), 16217-16228.
13. Cheng, C.; Truong, J.; Barrett, J. A.; Shen, D.; Abu-Omar, M. M.; Ford, P. C., Hydrogenolysis of Organosolv Lignin in Ethanol/Isopropanol Media without Added Transition-Metal Catalyst. *ACS Sustainable Chemistry & Engineering* **2019,** *8* (2), 1023-1030.
14. Zhou, M.; Sharma, B. K.; Li, J.; Zhao, J.; Xu, J.; Jiang, J., Catalytic valorization of lignin to liquid fuels over solid acid catalyst assisted by microwave heating. *Fuel* **2019,** *239*, 239-244.
15. Kong, L.; Liu, C.; Gao, J.; Wang, Y.; Dai, L., Efficient and controllable alcoholysis of Kraft lignin catalyzed by porous zeolite-supported nickel-copper catalyst. *Bioresource Technology* **2019,** *276*, 310-317.
16. Wu, Q.-y.; Ma, L.-l.; Long, J.-x.; Shu, R.-y.; Zhang, Q.; Wang, T.-j.; Xu, Y., Depolymerization of Organosolv Lignin over Silica-alumina Catalysts. *Chinese Journal of Chemical Physics* **2016,** *29* (4), 474-480.
17. Kong, L.; Zhang, L.; Gu, J.; Gou, L.; Xie, L.; Wang, Y.; Dai, L., Catalytic hydrotreatment of kraft

lignin into aromatic alcohols over nickel-rhenium supported on niobium oxide catalyst. *Bioresource Technology* **2020,** *299*, 122582.

18. Liu, S.; Lin, Z.; Cai, Z.; Long, J.; Li, Z.; Li, X., Selective depolymerization of lignosulfonate via hydrogen transfer enhanced in an emulsion microreactor. *Bioresource Technology* **2018,** *264*, 382-386.

19. Toledano, A.; Serrano, L.; Pineda, A.; Romero, A. A.; Luque, R.; Labidi, J., Microwave-assisted depolymerisation of organosolv lignin via mild hydrogen-free hydrogenolysis: Catalyst screening. *Applied Catalysis B: Environmental* **2014,** *145*, 43-55.

20. Huang, S.; Mahmood, N.; Tymchyshyn, M.; Yuan, Z.; Xu, C., Reductive de-polymerization of kraft lignin for chemicals and fuels using formic acid as an in-situ hydrogen source. *Bioresource Technology* **2014,** *171*, 95-102.

21. Zhao, W.; Li, X.; Li, H.; Zheng, X.; Ma, H.; Long, J.; Li, X., Selective Hydrogenolysis of Lignin Catalyzed by the Cost-Effective Ni Metal Supported on Alkaline MgO. *ACS Sustainable Chemistry & Engineering* **2019,** *7* (24), 19750-19760.

22. Luo, L.; Yang, J.; Yao, G.; Jin, F., Controlling the selectivity to chemicals from catalytic depolymerization of kraft lignin with in-situ H2. *Bioresource Technology* **2018,** *264*, 1-6.

23. Shu, R.; Zhang, Q.; Ma, L.; Xu, Y.; Chen, P.; Wang, C.; Wang, T., Insight into the solvent, temperature and time effects on the hydrogenolysis of hydrolyzed lignin. *Bioresource Technology* **2016,** *221* (17), 568-575.

24. Narani, A.; Chowdari, R. K.; Cannilla, C.; Bonura, G.; Frusteri, F.; Heeres, H. J.; Barta, K., Efficient catalytic hydrotreatment of Kraft lignin to alkylphenolics using supported NiW and NiMo catalysts in supercritical methanol. *Green Chemistry* **2015,** *17* (11), 5046-5057.

25. Sun, L.; Zhao, Y.; Gao, Z.; Yue, X.; Gao, S.; Gao, W.; Cheng, X.; Shang, N.; Wang, C., Highly Dispersed CoFe Catalyst for Selective Hydrogenation of Biomass-Derived Furfural to Furfuryl Alcohol. *Energy Technology* **2022,** *10* (2).

26. Sun, L.; Li, S.; Gao, Z.; Gao, S.; Gao, W.; Cheng, X.; Shang, N.; Gao, Y.; Wang, C., Selective hydrogenolysis of 5-hydroxymethylfurfural to 2,5-dimethylfuran over cobalt nanoparticle inlaid cobalt phyllosilicate. *Dalton Transactions* **2022,** *51* (8), 3096-3103.

27. Yue, X.; Zhang, L.; Sun, L.; Gao, S.; Gao, W.; Cheng, X.; Shang, N.; Gao, Y.; Wang, C., Highly efficient hydrodeoxygenation of lignin-derivatives over Ni-based catalyst. *Applied Catalysis B: Environmental* **2021,** *293*, 120243.

28. Zhang, L.; Shang, N.; Gao, S.; Wang, J.; Meng, T.; Du, C.; Shen, T.; Huang, J.; Wu, Q.; Wang, H.; Qiao, Y.; Wang, C.; Gao, Y.; Wang, Z., Atomically Dispersed Co Catalyst for Efficient Hydrodeoxygenation of Lignin-Derived Species and Hydrogenation of Nitroaromatics. *ACS Catalysis* **2020,** *10* (15), 8672-8682.

29. Dou, X.; Li, W.; Zhu, C., Catalytic hydrotreatment of Kraft lignin into liquid fuels over porous ZnCoOx nanoplates. *Fuel* **2021,** *283*, 118801.

30. Huang, X.; Koranyi, T. I.; Boot, M. D.; Hensen, E. J., Catalytic depolymerization of lignin in supercritical ethanol. *ChemSusChem* **2014,** *7* (8), 2276-88.

31. Huang, X.; Atay, C.; Korányi, T. I.; Boot, M. D.; Hensen, E. J. M., Role of Cu–Mg–Al Mixed Oxide Catalysts in Lignin Depolymerization in Supercritical Ethanol. *ACS Catalysis* **2015,** *5* (12), 7359-7370.

32. Yan, F.; Ma, R.; Ma, X.; Cui, K.; Wu, K.; Chen, M.; Li, Y., Ethanolysis of Kraft lignin to platform chemicals on a MoC1-x/Cu-MgAlOz catalyst. *Applied Catalysis B: Environmental* **2017,** *202*, 305-313.

33. Kong, X.; Liu, C.; Xu, W.; Han, Y.; Fan, Y.; Lei, M.; Li, M.; Xiao, R., Catalytic hydroprocessing of stubborn lignin in supercritical methanol with Cu/CuMgAlOx catalyst. *Fuel Processing Technology* **2021,**

218, 106869.

34. Stavila, V.; Foster, M. E.; Brown, J. W.; Davis, R. W.; Edgington, J.; Benin, A. I.; Zarkesh, R. A.; Parthasarathi, R.; Hoyt, D. W.; Walter, E. D.; Andersen, A.; Washton, N. M.; Lipton, A. S.; Allendorf, M. D., IRMOF-74(n)–Mg: a novel catalyst series for hydrogen activation and hydrogenolysis of C–O bonds. *Chemical Science* **2019,** *10* (42), 9880-9892.

35. Cheng, C.; Li, P.; Yu, W.; Shen, D.; Gu, S., Catalytic hydrogenolysis of lignin in ethanol/isopropanol over an activated carbon supported nickel-copper catalyst. *Bioresour Technol* **2021,** *319*, 124238.

36. Deuss, P. J.; Scott, M.; Tran, F.; Westwood, N. J.; de Vries, J. G.; Barta, K., Aromatic Monomers by in Situ Conversion of Reactive Intermediates in the Acid-Catalyzed Depolymerization of Lignin. *Journal of the American Chemical Society* **2015,** *137* (23), 7456-7467.

37. Szulejko, J. E.; Kim, Y. H.; Kim, K. H., Method to predict gas chromatographic response factors for the trace-level analysis of volatile organic compounds based on the effective carbon number concept. *J Sep Sci* **2013,** *36* (20), 3356-65.

38. Zhu, C.; Cao, J.-P.; Zhao, X.-Y.; Xie, T.; Zhao, M.; Wei, X.-Y., Bimetallic effects in the catalytic hydrogenolysis of lignin and its model compounds on Nickel-Ruthenium catalysts. *Fuel Processing Technology* **2019,** *194*, 106126.

39. A. Alejandre; F. Medina; X. Rodriguez; P. Salagre; Y. Cesteros; Sueiras, J. E., Cu/Ni/Al layered double hydroxides as precursors of catalysts for the wet air oxidation of phenol aqueous solutions. *Applied Catalysis B: Environmental* **2001,** *30*, 195-207.

40. Chen, G.; Xu, N.; Li, X.; Liu, Q.; Yang, H.; Li, W., Hydrogen production by aqueous-phase reforming of ethylene glycol over a Ni/Zn/Al derived hydrotalcite catalyst. *RSC Advances* **2015,** *5* (74), 60128-60134.

41. Wang, Y.; Wang, D.; Li, X.; Li, G.; Wang, Z.; Li, M.; Li, X., Investigation on the Catalytic Hydrogenolysis of Lignin over NbOx–Ni/ZnO–Al2O3. *Industrial & Engineering Chemistry Research* **2019,** *58* (19), 7866-7875.

42. Chen, J.; Li, Y.; Li, Z.; Zhang, X., Production of COx-free hydrogen and nanocarbon by direct decomposition of undiluted methane on Ni–Cu–alumina catalysts. *Applied Catalysis A: General* **2004,** *269* (1-2), 179-186.

43. Jing, K. Q.; Fu, Y. Q.; Chen, Z. N.; Zhang, T.; Sun, J.; Xu, Z. N.; Guo, G. C., Boosting Interfacial Electron Transfer between Pd and ZnTi-LDH via Defect Induction for Enhanced Metal-Support Interaction in CO Direct Esterification Reaction. *ACS Appl Mater Interfaces* **2021,** *13* (21), 24856-24864.

44. Lama, S. M. G.; Pampel, J.; Fellinger, T.-P.; Beškoski, V. P.; Slavković-Beškoski, L.; Antonietti, M.; Molinari, V., Efficiency of Ni Nanoparticles Supported on Hierarchical Porous Nitrogen-Doped Carbon for Hydrogenolysis of Kraft Lignin in Flow and Batch Systems. *ACS Sustainable Chemistry & Engineering* **2017,** *5* (3), 2415-2420.

45. A, N. K.; A, M. K.; B, M. A., Determining an optimum catalyst for liquid-phase dehydration of methanol to dimethyl ether. *Applied Catalysis A: General* **2008,** *349* (1–2), 6-12.

46. Verziu, M.; Tirsoaga, A.; Cojocaru, B.; Bucur, C.; Tudora, B.; Richel, A.; Aguedo, M.; Samikannu, A.; Mikkola, J. P., Hydrogenolysis of lignin over Ru-based catalysts: The role of the ruthenium in a lignin fragmentation process. *Molecular Catalysis* **2018,** *450*, 65-76.

47. Jeong, S.; Yang, S.; Kim, D. H., Depolymerization of Protobind lignin to produce monoaromatic compounds over Cu/ZSM-5 catalyst in supercritical ethanol. *Molecular Catalysis* **2017,** *442*, 140-146.

48. Ma, H.; Li, H.; Zhao, W.; Li, L.; Liu, S.; Long, J.; Li, X., Selective depolymerization of lignin catalyzed by nickel supported on zirconium phosphate. *Green Chemistry* **2019,** *21* (3), 658-668.

49. Wu, Z.; Zhang, J.; Zhao, X.; Li, X.; Zhang, Y.; Wang, F., Attapulgite - supported magnetic dual

acid – base catalyst for the catalytic conversion of lignin to phenolic monomers. *Journal of Chemical Technology & Biotechnology* **2019,** *94* (4), 1269-1281.

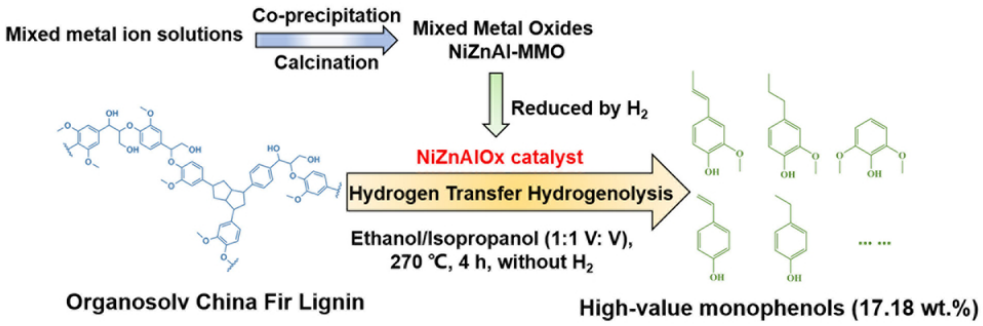

TOC

82x44mm (300 x 300 DPI)

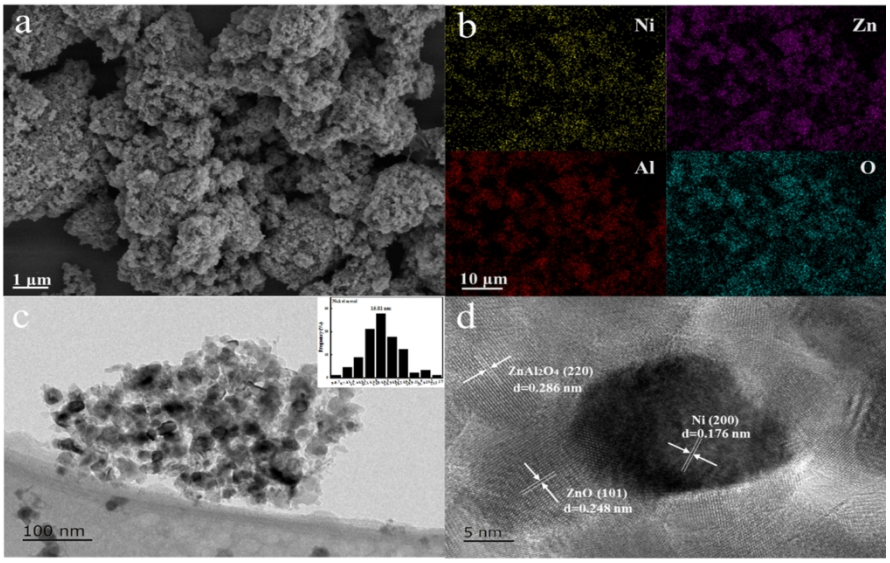

Figure 4 SEM image (a), SEM-mapping (b), TEM image (c) and Ni crystalline planes (b) of Ni3Zn7AlOx catalyst

209x284mm (300 x 300 DPI)

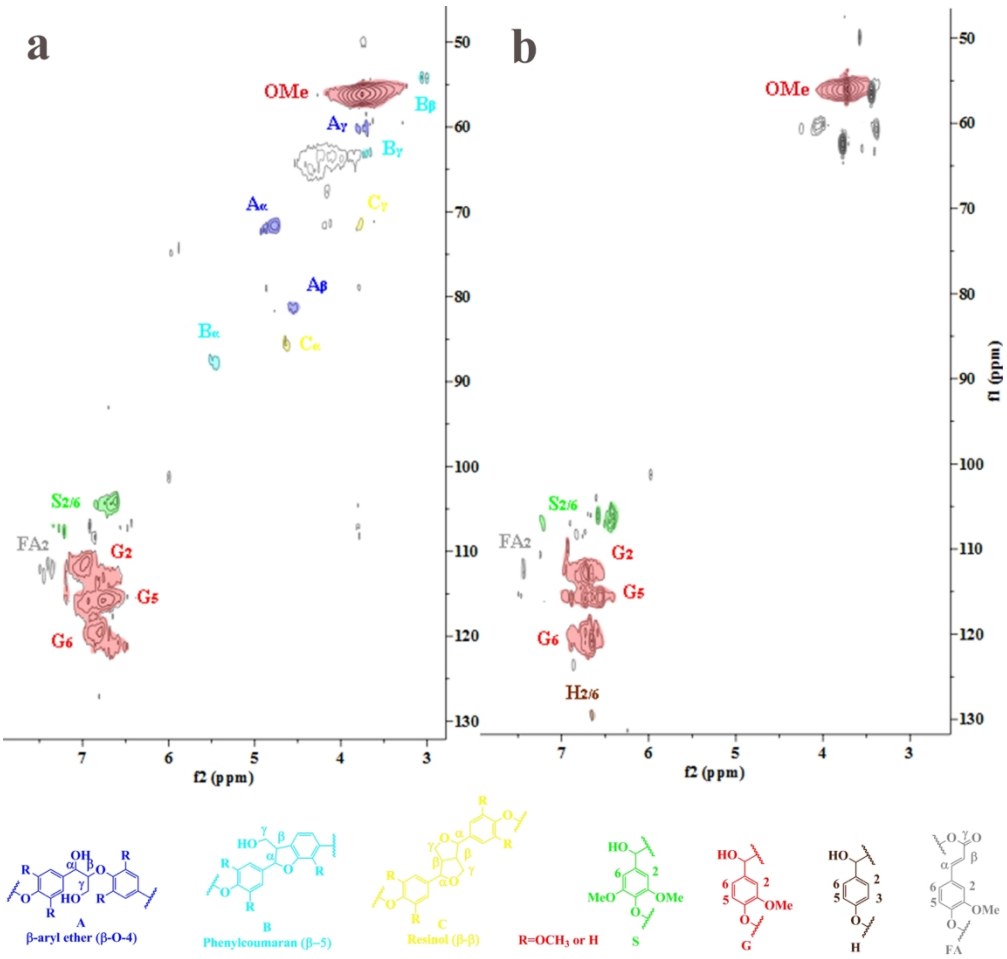

Figure 6 2D HSQC MNR of lignin (a) and bio-oil with the Ni3Zn7AlOx (b)

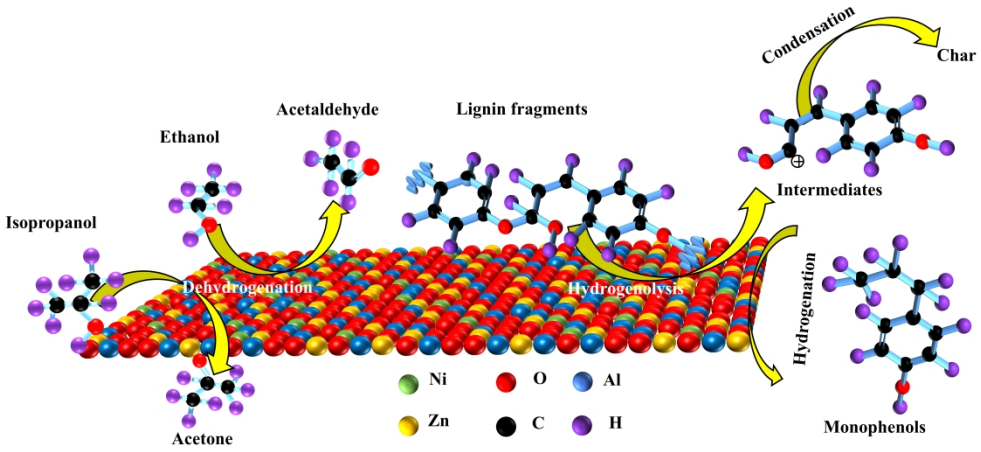

Figure 7 Plausible reaction pathways for the catalyzed hydrogenolysis of lignin

249x119mm (600 x 600 DPI)